

Structural Characterization, and Antioxidative and Anti-inflammatory Activities of Phylloxanthobilins in *Tropaeolum majus*, a Plant with Relevance in Phytomedicine[#]

OPEN
ACCESS

Authors

Patricia Frei¹, Christian Nadegger², Angelika M. Vollmar¹, Thomas Müller², Simone Moser^{1,3} 

Affiliations

- 1 Department of Pharmacy, Pharmaceutical Biology, Ludwig-Maximilian University of Munich, Germany
- 2 Institute of Organic Chemistry, University of Innsbruck, Austria
- 3 Institute of Pharmacy, Department of Pharmacognosy, University of Innsbruck, Austria

Key words

Tropaeolum majus, Tropaeolaceae, antioxidant, anti-inflammatory properties, phylloxanthobilins, pyro-phyllobilin, phytochemicals

received June 28, 2023
accepted after revision November 28, 2023

Bibliography

Planta Med 2024; 90: 641–650

DOI 10.1055/a-2225-8314

ISSN 0032-0943


© 2024. The Author(s).

This is an open access article published by Thieme under the terms of the Creative Commons Attribution-NonDerivative-NonCommercial-License, permitting copying and reproduction so long as the original work is given appropriate credit. Contents may not be used for commercial purposes, or adapted, remixed, transformed or built upon. (<https://creativecommons.org/licenses/by-nc-nd/4.0/>)

Georg Thieme Verlag KG, Rüdigerstraße 14,
70469 Stuttgart, Germany

Correspondence

Prof. Dr. Simone Moser
Institute of Pharmacy, Department of Pharmacognosy, University of Innsbruck, Center for Chemistry and Biomedicine
Innrain 80–82/IV, 6020 Innsbruck, Austria
Phone: + 4 35 12 50 75 84 00
Simone.Moser@uibk.ac.at

 Supplementary material is available under
<https://doi.org/10.1055/a-2225-8314>

ABSTRACT

Tropaeolum majus (garden nasturtium) is a plant with relevance in phytomedicine, appreciated not only for its pharmaceutical activities, but also for its beautiful leaves and flowers. Here, we investigated the phytochemical composition of senescent nasturtium leaves. Indeed, we identified yellow chlorophyll catabolites, also termed phylloxanthobilins, which we show to contribute to the bright yellow color of the leaves in the autumn season. Moreover, we isolated and characterized the phylloxanthobilins from *T. majus*, and report the identification of a pyro-phylloxanthobilin, so far only accessible by chemical synthesis. We show that the phylloxanthobilins contribute to bioactivities of *T. majus* by displaying strong antioxidative effects *in vitro* and *in cellulo*, and anti-inflammatory effects as assessed by COX-1 and COX-2 enzyme inhibition, similar to other bioactive ingredients of *T. majus*, isoquercitrin, and chlorogenic acid. Hence, phylloxanthobilins could play a role in the efficacy of *T. majus* in the treatment of urinary tract infections, an established indication of *T. majus*. With the results shown in this study, we aid in the completion of the phytochemical profile of *T. majus* by identifying additional bioactive natural products as relevant components of this medicinal plant.

Introduction

Lately, a chlorophyll-derived class of substances, PBs, has emerged as relevant among phytochemicals. PBs, known to accumulate in senescent leaves of vascular plants and peels of fruit,

[#] This work is dedicated to Professors Rudolf Bauer, Chlodwig Franz, Brigitte Kopp, and Hermann Stuppner for their invaluable contributions and commitment to Austrian Pharmacognosy.

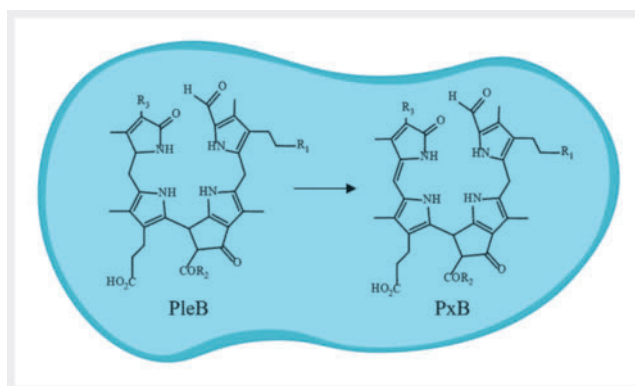
ABBREVIATIONS

CGA	chlorogenic acid
COX	cyclooxygenase
CP	chemically pure
FRAP	ferric reducing antioxidant power
IQ	isoquercitrin
LPS	lipopolysaccharide
NCC	nonfluorescent chlorophyll catabolite
PB	phyllobilin
PleB	phylloleucobilin
PxB	phyloxanthobilin
pyPxB	pyro-phyloxanthobilin
ROS	reactive oxygen species
RT	room temperature
TPTZ	2,4,6-tri(2-pyridyl)-s-triazine
YCC	yellow chlorophyll catabolite

have not been fully investigated yet [1]. Possessing tetrapyrrolic structures, they share structural similarities with bilirubin [2]. In some of the investigated plants, chlorophyll degradation leads to the formation of PxBs [also termed yellow chlorophyll catabolites (YCCs)] [3]. In terms of structure, PxBs are oxidation products of earlier discovered PleBs (or nonfluorescent chlorophyll catabolites (NCCs)) [1], from which PxBs are formed in the plant cell by a yet unclarified mechanism (► Fig. 1) [4]. A structural feature of naturally occurring PleBs is a carboxyl group or methyl ester function at ring E. The loss of the carboxyl function has not been discovered in plants yet; in ferns, however, so-called iso-phyllobilins feature a similar structural motif from a rearrangement reaction [5]. Semisynthetic approaches, however, achieved the formation of so-called pyro-PleBs (pyro-NCCs) by decarboxylation of natural PleBs using pig liver esterase and aqueous 20 mM H₂SO₄ at 80 °C for 6 h [6]. Contrary to the decarboxylation of PleBs, earlier intermediates in the breakdown of chlorophyll can easily decarboxylate; the reason for the stability of the carboxyl function of PleBs and PxBs in plants has not yet been revealed [5, 6].

Research in recent years has found that the breakdown of chlorophyll proceeds via a multistep biochemical pathway. Interestingly, the substances are formed in plants not only in autumn but also, e.g., in the event of a pathogen attack [1, 7]. This suggests that PBs could display plant protecting properties, as is known for other phytochemicals, such as flavonoids or saponins [8–10]. Data about chlorophyll, its derivatives, bioactivities, bioavailability, and antioxidative power is comprehensive [11]. For example, chlorophyllin, a sodium-copper salt analogue of chlorophyll, protects mitochondria against oxidative damage caused by reactive oxygen species (ROS), and membranes *in vitro* and *ex vivo* by inhibiting the generation of ROS [12].

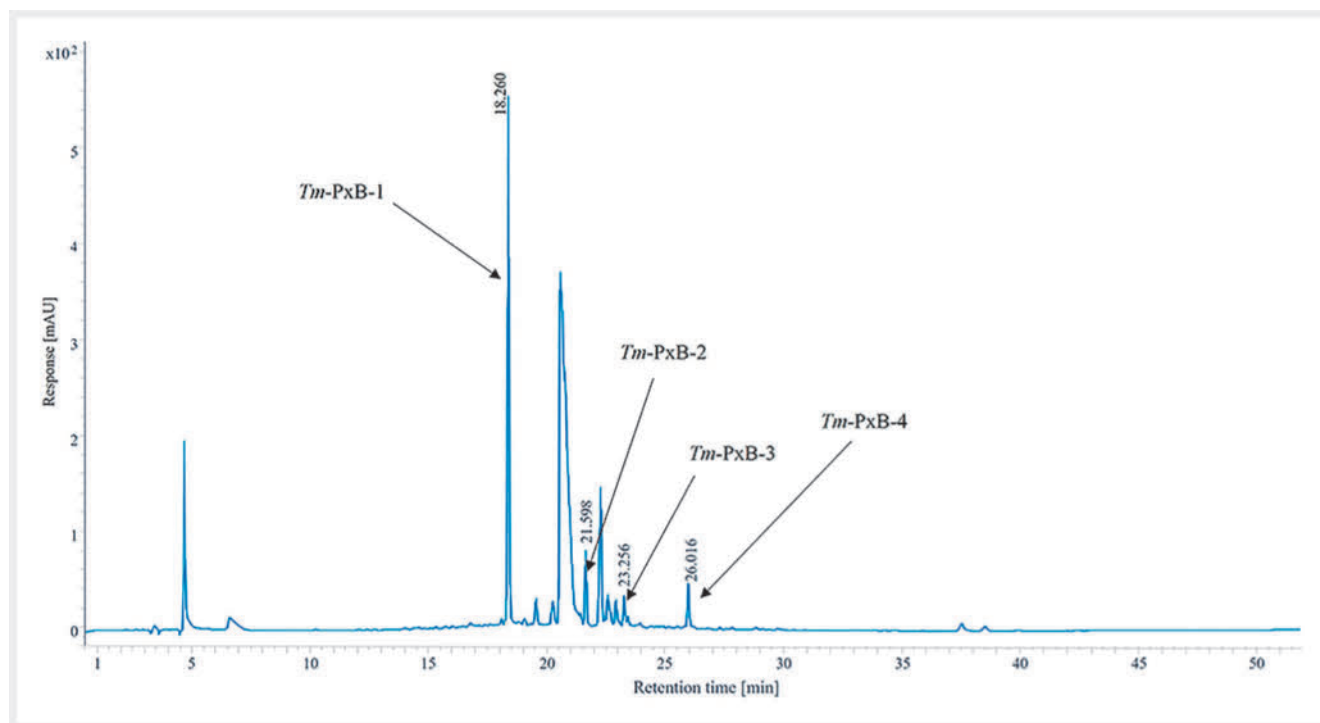
Regarding the products of the biochemical degradation of chlorophyll in the course of senescence, however, knowledge has only begun to accumulate recently. In order to render the identification of PBs in medicinal plants and food more straightforward, a PB spectral database has recently been published [13]. Current findings have shown that PxBs contained in food and medicinal



► Fig. 1 PleBs are oxidized to PxBs in plant vacuoles by a yet unclarified mechanism.

plants possess strong antioxidative activities. In *Echinacea purpurea*, a plant commonly used to treat the common cold, six PxBs were found with strong *in vitro* and *in cellulo* antioxidative activity [14]. Furthermore, a PxB from stinging nettle leaves was found to possess strong antioxidant power, considerably contributing to the plant's spectrum of activity [15]. Oxidative stress occurs as result of an imbalance between the generation and cleavage of radical oxygen species during various physiological processes, and is pathologically related to numerous diseases, such as atherosclerosis, diabetes, and Parkinson's disease [16–18]. Still, antioxidants are considered a promising tool to effectively conquer diseases [19]. Moreover, recent findings have pointed towards a suppressive potential of PBs on cellular immune activation pathways by inhibiting tryptophan catabolism to kynurenine in peripheral blood mononuclear cells (PBMCs), opening a complete view of the physiological effects of PBs [20].

Along these lines, the full characterization of the chemical components of *Tropaeolum majus* L. (garden nasturtium, Tropaeolaceae) remains incomplete, and the composition not only varies among different plant parts but is also influenced by cultivation methods and environmental conditions. The flowers represent the most analyzed part of the plant, and the phytochemical composition was found to be different depending on the color of the flowers [21]. In contrast, a limited number of studies have been conducted on nasturtium leaves, describing flavonoids, such as isoquercitrin, quercetin 3-glucoside, kaempferol, fatty acids, and glucosinolates, such as glucotropaeolin and sinalbin [21–24]. Garden nasturtium is widely cultivated and used as decorative food in, e.g., salads. In addition to the use as a food, nasturtium has also gained recognition in folk medicine for its diuretic and antibacterial effects. In Germany, *T. majus* is listed in the monographies of the commission E Nr. 162 of 1992 as phytomedicine in the treatment of urinary tract infections and catarrhs of the upper respiratory tract. Moreover, extracts of nasturtium leaves were reported by Gasparotto et al. to possess natriuretic and diuretic activity *in vivo*, and further, IQ is attributed as a bioactive key player of the multicomponent mixture [25]. Polyphenols, mainly CGA and ascorbic acid, were concluded to be the antioxidative and anti-inflammatory key players in herbal extracts of nasturtium [26].



► **Fig. 2** Analytical HPLC trace of acidified methanolic extracts of senescent *T. majus* leaves, detection at 420 nm, long HPLC method: mobile phase A = ammonium acetate buffer 10 mM pH 7, B = ACN, flow 0.5 mL/min. Solvent composition: 0–5 min 5% B, 5–45 min 5% to 60%, 45–51 min 60% to 100%, 51–53 min 100%, 53–55 min 100% to 5%.

In this study, we report the identification of four PxBs in leaves of *T. majus* that give rise to the yellow color of leaves during senescence and possess strong antioxidant and anti-inflammatory potency comparable to CGA and IQ; hence, PxBs from nasturtium leaves may contribute to the effects of nasturtium as a medicinal plant. In addition, we uncover the first natural source of a pyPxB, which opens the door for investigating the bioactivities of an interesting structural motif.

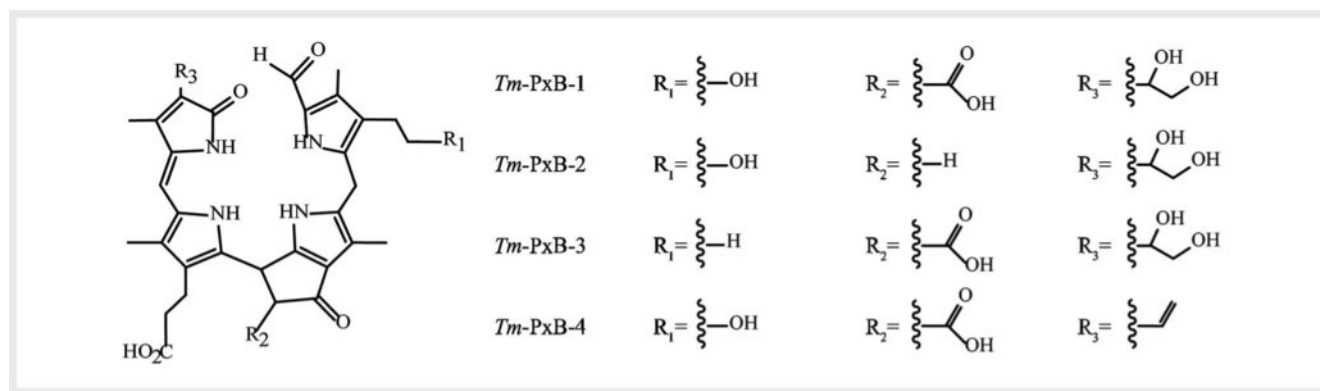
Results and Discussion

Investigating the constituent fingerprint of aqueous methanolic extracts of *T. majus* leaves by analytical HPLC, four different PxBs were identified by their characteristic UV spectrum (► **Fig. 2**) [13]. As widely established for PBs, PxBs were named by the botanical source (prefix) and numbered *Tm*-PxB-(1–4) according to decreasing polarity. The characteristic UV/Vis spectrum of PxB has an absorbance maximum at 426 nm, which is due to rings A to D possessing an extended π -electron system and carrying a vinyl residue at ring D [3]. *Tm*-PxB-4, being the less polar, was detected to have maxima at 430, 314, and 246 nm. *Tm*-PxB-(1–3) showed a shifted maximum to a lower wavelength at 418 nm, besides the maxima at 314–316 nm and 242–246 nm, which was reported earlier for PxBs of which the vinyl group is replaced by a dihydroxyethyl residue at ring D in *Egeria densa* and *E. purpurea* (**Fig. 2S**, Supporting Information) [14, 27].

Relative content of PxBs in methanolic extracts of fresh yellow leaves to the sum of all peak areas in the 420 nm HPLC trace

yielded a total of approximately 25% (**Figs. 3S and 4S**, Supporting Information). Since the yellow color is widely associated with the wavelength at 420 nm, it can be concluded that PxBs are responsible for an estimated 25% of the yellow coloration of nasturtium leaves in autumn.

For the structural elucidation of PBs, a total of 200 g of senescent leaves were used for extraction, as described in the “General experimental procedures” section. The yield amounted to 12.3 mg of *Tm*-PxB-1, 0.8 mg of *Tm*-PxB-2, 1.1 mg of *Tm*-PxB-3, and 2.3 mg of *Tm*-PxB-4, as quantified by UV/Vis spectroscopy. HR-ESI-MS was performed to identify the elemental composition, and MS² experiments were performed to elucidate side chain modifications via the characteristic fragmentation reactions according to Müller et al. [28]. The molecular formulae were derived from the $[M - H]^-$ as well as $[M + H]^+$ molecular ions to be C₃₄H₃₈N₄O₁₀ for *Tm*-PxB-1, C₃₃H₃₈N₄O₈ for *Tm*-PxB-2, C₃₄H₃₉N₄O₉ for *Tm*-PxB-3, and C₃₄H₃₆N₄O₈ for *Tm*-PxB-4. Further MS² experiments in the positive ion mode revealed characteristic fragmentations for all four PxBs, namely, the loss of H₂O, CO₂, as well as cleavages at the saturated meso positions between rings A and B as well as rings B and C (**Figs. 6S–9S**, Supporting Information). Additionally, matching of databases indicated that *Tm*-PxB-1 may be the corresponding oxidation product of *So*-PleB-1 (*So*-NCC-1) of spinach, also known as *Mc*-PleB-26 (*Mc*-NCC-26), the most polar PleB found in ripening peels of banana [29–31]. To further verify the proposed structure, fresh spinach extracts were analyzed by HPLC. HPLC analysis revealed identical retention times of *So*-PleB-1 and the corresponding PleB in the nasturtium



► **Fig. 3** Chemical structure of the *Tm*-PxB core and side chain modifications.

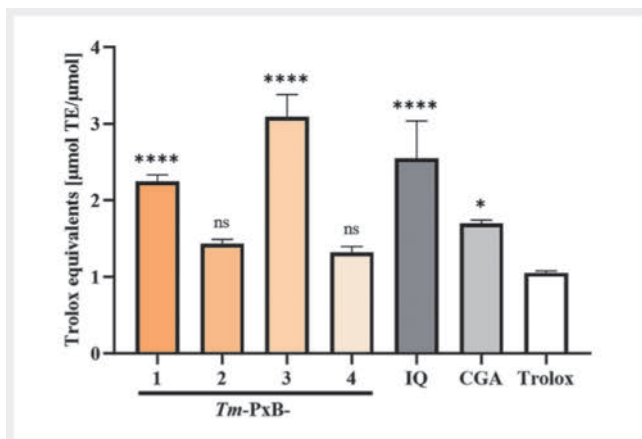
extract, indicating that a catabolite identical to *So*-PleB-1 is present in nasturtium leaves (**Fig. 5S**, Supporting Information).

In addition to MS² fragmentations that already provided information on the molecular structures (► **Fig. 3**), ¹H-NMR spectra as well as homo- and heteronuclear 2D spectra (COSY, ¹H,¹³C-HMQC, ¹H,¹³C-HMBC) were acquired for *Tm*-PxB-1 and *Tm*-PxB-4 for further confirmation (**Figs. S11–S15**, Supporting Information). The ¹H-NMR spectra of *Tm*-PxB-1 and *Tm*-PxB-4 showed a set of typical signals for PBs. Among them were four characteristic signals around 2 ppm assigned to the methyl groups, as well as a characteristic signal at 9.5 ppm originating from the formyl group. The double bond between C15 and C16, a decisive factor for the yellow color of PxBs, was displayed by a signal at 5.96 ppm (*Tm*-PxB-1) and 6.04 ppm (*Tm*-PxB-4), respectively. While the spectrum of *Tm*-PxB-4 showed characteristic signals for a vinyl group at 5.26/6.32 and 6.50 ppm, these signals were replaced by high shifted signals, characteristic for the dihydroxy side chain of *Tm*-PxB-1 (**Table 1S**, Supporting Information). For *Tm*-PxB-2, ¹H-NMR spectra were recorded (**Fig. 13S**, Supporting Information). Although only some of the characteristic signals could be assigned, a typical pattern for PxBs became evident; the four methyl groups showed singlets at 2.16, 1.98, 2.06, and 2.15 ppm. The protons of the dihydroxy side chain at C18 showed signals at 4.47 ppm and 3.46/3.68 ppm, respectively. Signals from pyrrole nitrogen-bound protons were visible at around 10 ppm, and the proton at C15 manifested in a signal at 5.98 ppm, supporting the presence of a double bond. In summary, results of ¹H-NMR as well as tandem MS analyses strengthened *Tm*-PxB-2 to be a pyPxB-type chlorophyll degradation product (► **Fig. 3**).

To test whether the newly discovered pyPxB is formed during the extraction process and therefore is a possible degradation product of *Tm*-PxB-1, the stability of this PxB in different media that were used during extraction was tested by HPLC analysis. Indeed, *Tm*-PxB-1 was stable for 1 h of incubation at RT and still accounted for 100% in PBS pH 7 and PBS 5.2. Samples acidified with AcOH (pH 3.5), when left at RT overnight, showed a reduction of the *Tm*-PxB-1 peak area of 22% and 4% formation of *Tm*-PxB-2, 0.3% of *Tm*-PxB-3, and 1.6% of *Tm*-PxB-4. The behavior of *Tm*-PxB-1 in acidic PBS pH 2.5 overnight was additionally analyzed by LC-MS. The peak area of *Tm*-PxB-1 diminished overnight in ac-

idified PBS pH 2.5 by 18%, accompanied by a rise to 4% of the signals for *Tm*-PxB-2, 1.3% of *Tm*-PxB-3, and 0.7% of *Tm*-PxB-4, respectively. *Tm*-PxB-1 degraded partially to the other three PxBs, most likely by decarboxylation and dehydrogenation in acidic conditions. Therefore, the formation of the pyPxB could be a result of degradation of *Tm*-PxB-1 during acid extraction processes. To exclude *Tm*-PxB-2 to be an artefact of purification, freshly harvested senescent nasturtium leaves were investigated under ambient MS conditions using leaf spray ionization (**Fig. 16S**, Supporting Information). In Leaf Spray MS, leaf samples are cut prior to analysis and placed directly in front of the ion source, which allows for the direct analysis of the leaf composition and to answer the question, which of the identified PxBs were native ingredients of the plant [32, 33]. Using this method, all four PxBs were detected, with *Tm*-PxB-1 being the most abundant. Sodium adducts of *Tm*-PxB-2 accounted for 92%, *Tm*-PxB-3 for 9%, and *Tm*-PxB-4 for 67% of signal intensities, related to the intensity of [M + Na]⁺ *Tm*-PxB-1. For *Tm*-PxB-2, besides an [M + Na]⁺ ion, also [M + K]⁺ and [M + 2K]⁺ adducts were found; this experiment provides evidence that *Tm*-PxB-2 is indeed a genuine ingredient of nasturtium leaves.

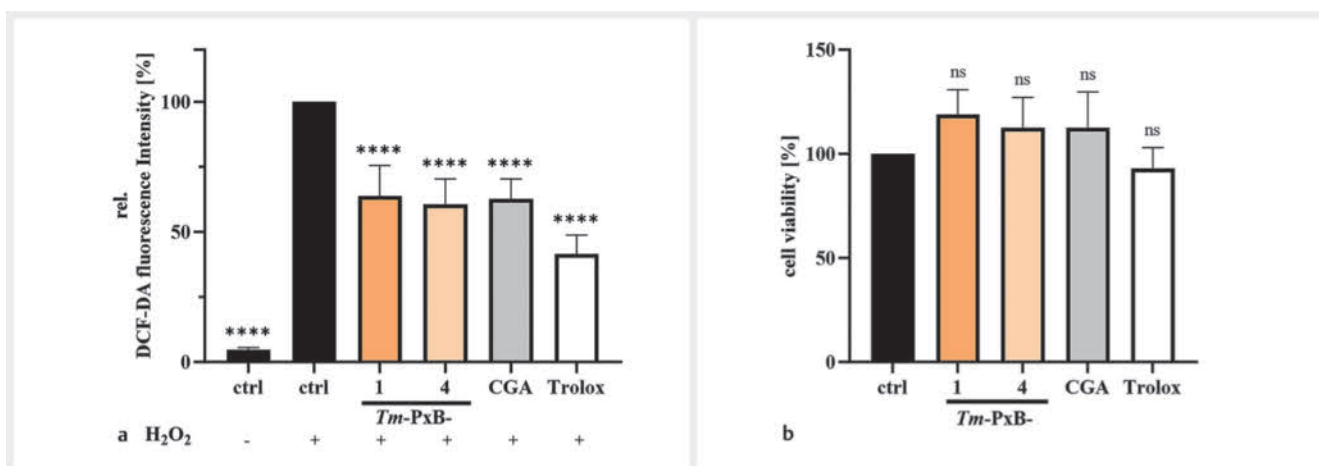
The *in vitro* antioxidative potential of the characterized *Tm*-PxBs was assessed by a FRAP assay (► **Fig. 4**). This assay measures the iron reducing ability of antioxidants, and antioxidant power correlates to the formation of the Fe²⁺-(TPTZ)₂ complex, which can be quantified at 593 nm using a Trolox standard curve. *Tm*-PxB-1 and *Tm*-PxB-3 significantly possessed stronger antioxidative activities relative to Trolox, with *Tm*-PxB-1 displaying two times higher and *Tm*-PxB-3 three times higher activities than the vitamin E derivative Trolox. *Tm*-PxB-2 and *Tm*-PxB-4 exhibited comparable antioxidative strength compared to Trolox. CGA and IQ are known polyphenolic ingredients of nasturtium leaves. Both exhibited stronger effects than Trolox and were in the same range as for the tested PBs and in accordance with the literature (NCCs) [34, 35]. To further investigate the antioxidative effects of PxBs from nasturtium *in cellulo*, a ROS assay was performed for selected PBs (► **Fig. 5a**). The conversion of an intracellular dye in response to H₂O₂ represents a readout for ROS. Radical scavengers are known for their ability to reduce intracellular ROS production. Demonstrated for *Tm*-PxB-1 and *Tm*-PxB-4 in low micromolar concentrations, a reduction of 36% was observed for *Tm*-PxB-1, while with



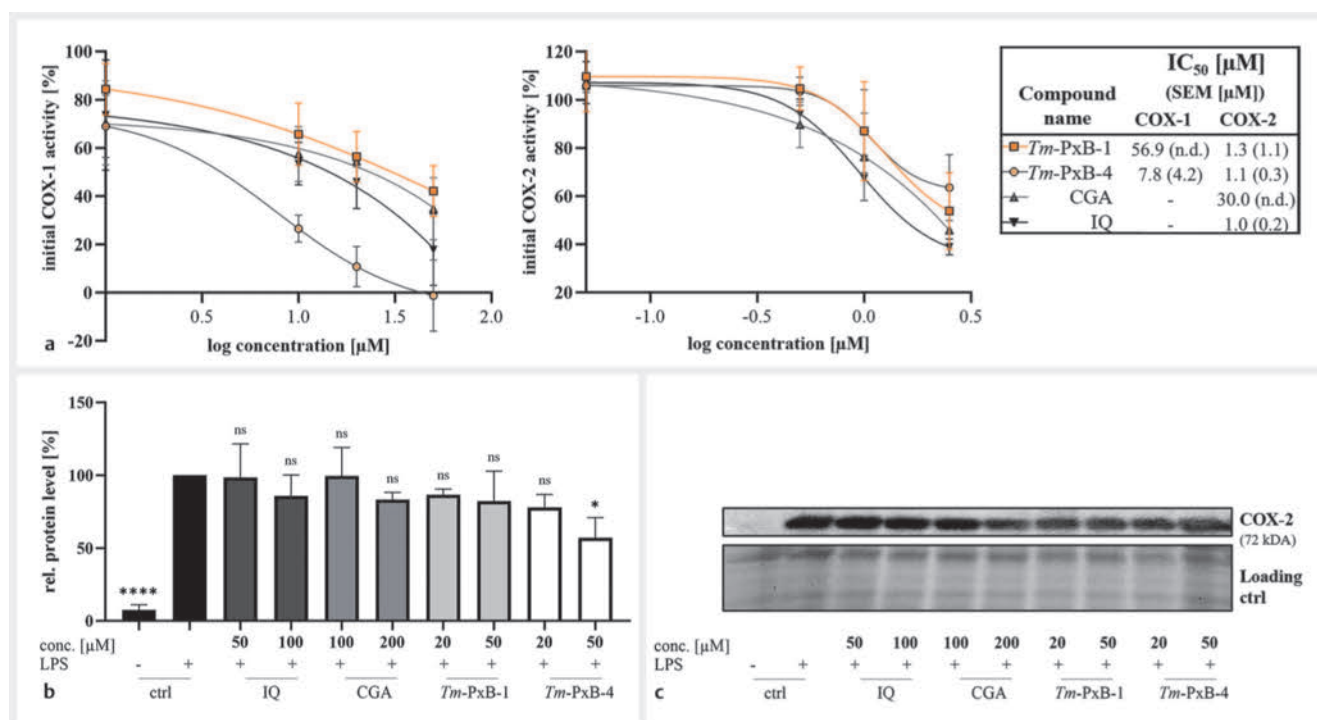
► **Fig. 4** PxBs possess strong antioxidative potential *in vitro*, as assessed by a FRAP assay. Expressed as Trolox equivalents ($\mu\text{mol TE}/\mu\text{mol}$), *Tm*-PxB-1 and *Tm*-PxB-3 showed 2- and 3-fold higher antioxidative power, respectively, and *Tm*-PxB-2 and *Tm*-PxB-4 were comparable to Trolox. CGA and IQ, known ingredients of *Tropaeolum*, also exhibited significantly stronger activity than Trolox. Values represent the mean \pm standard deviation of three independent experiments with three replicates each (ns = not significant, * $p < 0.05$, **** $p < 0.0001$).

Tm-PxB-4, a reduction of 39% of ROS production was achieved relative to the positive control (H_2O_2 -treated cells). CGA inhibited ROS production in a comparable manner by 37%. To exclude an influence of the substances on cell viability and therefore also ROS production, cell viability was also assessed. No significant influence on cell viability due to the treatment of the cells with substances was found (► **Fig. 5 b**).

Urinary tract infections are among the indications of *T. majus* and are mainly attributed to the antibacterial potency of isothiocyanates; therefore, a combination of enriched extracts of nasturtium herb and horseradish roots is commonly used for treatment [36]. Inhibiting the inflammatory cascade by substances of nasturtium via COX-1 and COX-2 can aid in our understanding of the effects elicited by nasturtium in the treatment of cystitis. Investigating the influence of *Tm*-PxB-1 and *Tm*-PxB-4 on COX-1 and COX-2 activity, both exhibited inhibitory effects in low micromolar concentrations, similar to CGA. While for both, *Tm*-PxB-1 and *Tm*-PxB-4, an inhibition of COX-2 with an IC_{50} below $10 \mu\text{M}$ was observed, *Tm*-PxB-1 inhibited COX-1 with an IC_{50} above $50 \mu\text{M}$, and *Tm*-PxB-4 with an IC_{50} of $8 \mu\text{M}$. The IC_{50} of CGA on COX-2 was $30 \mu\text{M}$ and $1 \mu\text{M}$ for IQ. For COX-1, no IC_{50} value could be calculated for neither IQ nor CGA. Comparing COX-1 activity dose-response curves of PxBs to CGA and IQ, only *Tm*-PxB-4 exhibited a pronounced inhibition of COX-1, with an IC_{50} of $8 \mu\text{M}$. Moreover, IC_{50} values on COX-2 inhibition showed a comparable effect of IQ and PxBs, and a presumable stronger inhibitory potential than CGA (► **Fig. 6 a**). On the protein level, *Tm*-PxB-4 significantly diminished COX-2 expression in LPS-stimulated macrophages, as shown earlier for a PxB from *Urtica dioica* [15]. In contrast, for CGA, IQ, and *Tm*-PxB-1, no significant influence on COX-2 expression was found (► **Fig. 6 b, c**). Cell viability was measured for all samples and showed that compound treatment did not affect cell viability at the tested concentrations (**Figs. 175** and **185**, Supporting Information). *T. majus* L. herb has been reported to possess inhibitory effects on the activity of COX-1 [26]. Further investigations on the constitution of the herb extracts responsible for COX-1 inhibition and possible effects on COX-2 have not been examined yet. IQ as an active flavonoid is known for its inhibitory potential against mainly COX-2 [37]. Its ability to downregulate COX-1 activity has only been shown for high concentrations, resulting



► **Fig. 5** PxBs of *T. majus* scavenge ROS in HeLa cells (a) without influencing cell viability (b). a Cells were stimulated with the compound ($10 \mu\text{M}$, Trolox 1 mM) for 24 h, then treated with dye (30 min) and H_2O_2 (30 min). Radical scavenging activity was measured as the ability to prevent the conversion of the dye H_2DCF to fluorophore DCF. b *Tm*-PxB-1, *Tm*-PxB-2, Trolox, and CGA did not affect cell viability at $10 \mu\text{M}$ (1 mM for Trolox). Cell viability was tested after 24 h by a crystal violet staining after stimulation of the compounds under the same conditions. For relative quantification, the mean of control triplicates was set to 100% for each repetition. Values represent the mean \pm standard deviation of four independent experiments performed in duplicate (ctrl = control, ns = not significant, **** $p < 0.0001$).



▶ Fig. 6 *In vitro* dose-dependent inhibition of COX-1 and COX-2 activity by *Tm*-PxB-1, *Tm*-PxB-4, CGA, and IQ. For IC₅₀ determination, data of three independent experiments were calculated as percentages of the initial activities and normalized to the positive control with 100% activity. Error bars represent the mean ± SEM (n. d. = SEM was not calculated because of a poor fit of the nonlinear regression). **b**, **c** COX-2 expression of LPS and compound-stimulated J774A.1 macrophages. For determination of COX-2 expression, cells were stimulated with LPS (0.5 μg/mL), and compounds, as indicated, for 4 h before cell lysis and Western blotting. **b** Quantitative analysis of COX-2 protein levels was normalized to the whole lane protein and was calculated relative to the LPS-stimulated control. Values represent the mean ± standard error of the mean of three independent experiments (ns = not significant, * *p* < 0.05, **** *p* < 0.0001). **c** One representative example is shown.

in IC₅₀ values above 100 μM [38]. By discovering further potent COX-1 and, in particular, COX-2 inhibitors in nasturtium leaves, PxBs expand the phytochemical repertoire of this medicinal plant.

The catabolites accumulating due to the programmed degradation of chlorophyll, the PBs, have long been regarded as irrelevant side products of a detoxification process. Research of the last few years, however, shows a different picture. In particular, yellow chlorophyll catabolites, PxBs, have emerged as interesting bioactive natural products, which are relevant ingredients of medicinal plants. Investigating *T. majus*, we identified four PxBs, among which one was determined as a pyro-PxB lacking a carboxyl function. We further show that these PxBs can interconvert under acidic conditions. Using leaf spray MS, however, we show that all four identified PxBs occur genuinely in the plant. Moreover, we demonstrate bioactivities related to the use of *T. majus* in phyto-medicine, i.e., antioxidative and anti-inflammatory activities. The identification and investigation of PxBs in *T. majus* is another important step in establishing an overlooked family of natural products, the PBs, as relevant phytochemicals in medicinal plants.

Material and Methods

General experimental procedures

NMR spectra were recorded on an Avance III HD 500 MHz NMR spectrometer from Bruker BioSpin equipped with a CryoProbe Prodigy broadband probe using *d*₆-DMSO as the solvent. Data were processed using MestreNova 14.1.1.

ESI-MS and MS²: HR-MS were measured in the LMU Department of Chemistry MS facility; data were processed with Xcalibur 4.1 from Thermo Scientific. MS² fragmentations and leaf spray mass spectrometry were measured using a Thermo Scientific Q Exactive mass spectrometer and generated with Xcalibur 4.1 and mMass [39].

Analytical HPLC analysis was performed using either a short or long method for crude extracts with an Agilent 1260 Infinity II LC system with a 1260 Infinity degasser, an 1100 series quaternary pump, an 1100 series diode array detector, and an Agilent Poroshell column 120EC-C18 4 μm 4.6 × 150 mm with a connected Phenomenex ODS 4 × 3 mm i. d. pre-column. The injection volume was 100 μL. The solvent system for long method was mobile phase A = ammonium acetate buffer 10 mM pH 7, B = ACN, flow 0.5 mL/min. Solvent composition was 0–5 min 5% B, 5–45 min 5% to 60%, 45–51 min 60% to 100%, 51–53 min 100%,

53–55 min 100% to 5%. The short method was used for pure samples or intermediate check up with a solvent system: mobile phase A = ammonium acetate buffer pH 10 mM pH 7, B = ACN, flow 0.5 mL/min, and solvent composition 0–2 min 5% B, 2–17 min 5% to 100%, 17–20 min 100%, 20–22 min 100% to 5%.

Semipreparative HPLC was carried out using a Büchi Pure C-830 with a prep HPLC pump 300 bar, fraction collector, prep sample injection valve, and diode array detector. The column was a Luna C18, 5 μ m, 250 mm \times 21.2 mm, with a Phenomenex pre-column C18 15 \times 21.2 mm and the method comprised mobile phase A = phosphate buffer 0.02 M, pH 7, B = MeOH, flow 18 mL/min with solvent composition 0–5 min 15% B, 5–10 min 15% to 30% B, 10–40 min 30% to 55% B, 40–42 min 55% to 100% B.

Low-resolution LC-MS was conducted using an Agilent 1100 SL system (G1313A ALS, G1316A COLCOM, G1316A VWD, G1312A Bin Pump) coupled to a Bruker Daltonik HCTUltra PTM Discovery system (ESI mode). An Agilent Poroshell column 120EC-C18 4 μ m 4.6 \times 150 mm with connected Phenomenex ODS 4 \times 3 mm i. d. pre-column was used. Solvents were degassed in an ultrasonic bath and samples filtered by a PTFE syringe filter (\emptyset 0.45 μ m). Gradient consisted of A = water + 0.1% FA, B = ACN + 0.1% FA, flow 0.5 mL/min, with a solvent composition of 0–2 min 5% B, 2–17 min 5% to 100% B.

DMSO stocks of isolated substances were prepared from isolated or purchased substances and stored at -20°C . Concentrations of *Tm*-PxBs were calculated by $\log \epsilon$ (426 nm) = 4.51, PleB by $\log \epsilon$ (312 nm) = 4.23 using a Thermo Spectronic Genesys 5 (336001) UV-Visible spectrophotometer, λ_{max} [nm] (ϵ_{rel}) [3, 4]. Peak purity was tested using Agilent OpenLab CDS software [UV peak purity (p) in parts per million]: *Tm*-PxB-1 p = 999.42; *Tm*-PxB-2 p = 867.07; *Tm*-PxB-3 p = 996.67; *Tm*-PxB-4 p = 999.86. Varying peak purity is a result of an intrinsic 8²-epimerization of PBs [40], as observed for *Tm*-PxB-2.

HPLC grade MeOH, EtOH, acetonitrile (MeCN), and HCl were purchased from VWR International GmbH, and ultrapure water (18 M Ω \cdot cm⁻¹) was from a Millipore S.A.S Milli-Q Academic system (18.2 M Ω \cdot cm⁻¹). *d*₆-DMSO was obtained from Eurisotop, hydrogen peroxide (30%) from Bernd Kraft, TPTZ, iron(III) chloride (FeCl₃), and isoquercitrin (purity 98.2%, CP) were from Merck. Chlorogenic acid (purity 98.3%, HPLC) and DMSO (purity \geq 99.99%, GC) were from Carl Roth. Accutase and LPS were from Sigma-Aldrich. Trolox (purity 100%, HPLC) was from Cayman chemical and 2',7'-dichlorodihydrofluorescein diacetate (H₂DCF-DA) was from Thermo Fisher. COX Fluorescent Inhibitor Screening Kit was from Cayman Chemicals and SepPak Plus C18 cartridges from Waters Associates. DMEM medium was from PAN-Biotech and fetal calf serum (FCS) was from PAA Laboratories GmbH. COX-2 monoclonal antibody was purchased from Transduction Laboratories and peroxidase conjugated secondary antibody was from abcam. Cell culture. HeLa cells were obtained from the Deutsche Sammlung von Mikroorganismen und Zellkulturen (DSMZ) and cultured in DMEM medium supplemented with 10% FCS. J774A.1 cells were a kind gift from Prof. Veit Hornung from the Gene Center Munich and were cultivated in DMEM supplemented with 10% FCS and 1% sodium pyruvate. Both cell lines were cultivated at 37 $^{\circ}\text{C}$ under a 5% CO₂ atmosphere and split in a 1 : 10 ratio every 3 to 4 days.

Plant material

Senescent fresh leaves of *T. majus* were collected in the botanical garden of Munich-Nymphenburg (accession number F/0225, determined by Dr. Andreas Gröger, curator of the Botanical Garden Munich-Nymphenburg) and stored at -20°C until further use. Spinach (*Spinacia oleracea*) was purchased from a local supermarket.

Extraction and isolation of *Tm*-PxBs from fresh senescent leaves

PBs were isolated as described earlier according to Karg et al. [14] with minor adjustments. In brief, 100 g of frozen senescent leaves were ground with 250 mL of extraction mixture consisting of 60% MeOH, 40% PBS 50 mM pH 5.2 using a Braun hand blender Model MR 5000 in a 1000-mL beaker. The mixture was incubated at RT in the dark for 1 h, then filtered through a pleated filter paper with a \emptyset of 400 mm. The solid residue was washed twice with 200 mL of solvent mixture and filtered again. With the addition of 50% AcOH, the solution was acidified to pH 3.5 and stirred at RT in the dark overnight. Before further purification with semipreparative HPLC, the extract was concentrated to 20 mL, centrifuged (1000 g, 5 min), and filtered. The procedure was repeated for another 100 g of leaves. Fractions containing PBs were combined and repurified by semipreparative HPLC after evaporating and redissolving in 20/80 MeOH/potassium phosphate buffer 100 mM pH 7. The purity of isolated PBs was confirmed by analytical HPLC, then the compounds were dissolved in ACN/potassium phosphate buffer (pH 2.5) 20/80 and stirred overnight. Using SPE (Sep-Pak-C18 cartridge 5 g), pure PBs were eluted with ACN and lyophilized. The stability of the purified compound after acidifying was controlled by HPLC. For further use, DMSO stocks were prepared and stored at -20°C .

Chemoprofiling of *Tropaeolum majus* leaves

A piece of approximately 1 cm² each of four different yellow leaves of *T. majus* was cut out (Fig. 2S, Supporting Information) and ground with 200 μ L of MeOH in a mortar, diluted 1 : 11 with potassium phosphate buffer 100 mM pH 7 (20/80), and centrifuged. A 100- μ L portion of the extract was analyzed by analytical HPLC. PxBs were assigned by their UV/Vis spectra from a diode array detector, and their relative content was assessed by their HPLC peak areas relative to the sum of the peak areas at 420 nm.

Spectroscopic data

MS/MS fragmentation is presented below; further spectroscopic data is presented in detail in the Supporting Information.

MS/MS *Tm*-PxB-1 (hcd10): *m/z* (%) = 663.27 (5, [M + H]⁺, C₃₄H₃₉O₁₀N₄⁺); 645.25 (75, [M + H-H₂O]⁺); 627.24 (32, [M + H-H₂O-H₂O]⁺); 601.26 (100, [M + H-H₂O-CO₂]⁺);

MS/MS *Tm*-PxB-2 (hcd14): *m/z* (%) = 619.26 (2, [M + H]⁺, C₃₃H₃₉O₈N₄⁺); 601.27 (100, [M + H-H₂O]⁺); 583.26 (4, [M + H-H₂O-H₂O]⁺);

MS/MS *Tm*-PxB-3 (hcd10): *m/z* (%) = 647.27 (5, [M + H]⁺, C₃₄H₃₉O₉N₄⁺); 629.26 (56, [M + H-H₂O]⁺); 611.25 (34, [M + H-H₂O-H₂O]⁺); 585.27 (100, [M + H-H₂O-CO₂]⁺);

MS/MS *Tm*-PxB-4 (hcd10): m/z (%) = 629.26 (71, [M + H]⁺, C₃₄H₃₇O₈N₄⁺); 611.25 (62, [M + H-H₂O]⁺); 585.27 (100, [M + H-CO₂]⁺).

Comparison of retention times

A fresh spinach leaf was ground with 200 μ L of MeOH in a mortar, diluted 1 : 11 with potassium phosphate buffer 100 mM pH 7 (20/80), and centrifuged. A DMSO stock of isolated PleB was diluted in phosphate buffer 100 mM pH 7 (20/80). Samples were analyzed by analytical HPLC.

Leaf spray

Leaf spray analysis was performed according to a published protocol with minor modifications using a Thermo Scientific Q Exactive [41]. Yellow senescent leaves were freshly collected and cut into triangles using scissors. The tips of the leaf triangles were mounted in front of the MS inlet. During the measurement, approx. 10 μ L of MeOH were dropped onto the leaf triangles several times.

Stability of *Tm*-PxB-1 in extraction solvents

To test the stability of *Tm*-PxB-1 during extraction processes, *Tm*-PxB-1 was dissolved in either PBS of different pH values (pH 7/5.2/2.5) or AcOH (pH 3.5), and peak areas were analyzed by analytical HPLC after 1 h or 24 h of incubation at RT. Relative peak areas were calculated relative to HPLC peak areas of freshly prepared *Tm*-PxB-1 in PBS pH 7, which was immediately injected. PxBs were identified by their UV spectrum and retention times. *Tm*-PxB-1 samples in PBS pH 2.5 overnight were additionally analyzed by LC-MS.

Biological assays

Ferric reducing antioxidant potential assay

The FRAP assay was performed as described by Karg et al. [14] with minor modifications. Briefly, freshly prepared FRAP reagent was added to 100 μ M of compounds and different concentrations of Trolox for 5 min at 37 °C in a 96-well plate. The FRAP reagent consisted of 10 vol 300 mM acetate buffer pH 3.6, 1 vol 10 mM TPTZ in 40 mM HCl and 1 vol 20 mM iron(III) chloride. Antioxidants reduced the Fe³⁺-(TPTZ)₂ complex to intense blue Fe²⁺-(TPTZ)₂ complex with an absorption maximum at 593 nm. A calibration curve was established by measuring the absorbance of different Trolox concentrations. The antioxidant power of the compounds was calculated relative to Trolox and expressed as Trolox equivalents.

In cellulo reactive oxygen species assay

The intracellular ROS assay was conducted according to Karg et al. [14]. In short, 1 \times 10⁵ HeLa cells/mL in 100 μ L were seeded in 96-well plates and preincubated for 24 h. After treatment with *Tm*-PxB-1 (10 μ M), *Tm*-PxB-4 (10 μ M), CGA (10 μ M), Trolox (1 mM), or DMSO control for 24 h, the medium was removed, H₂DCF-DA (10 μ M) was added, and the plate was incubated for 30 min. After washing with PBS, cells were incubated with hydrogen peroxide (1 mM) for 30 min, and the formation of a highly fluorescent 2',7'-dichlorofluorescein (DCF) by intercellular oxidation of H₂DCF-DA was measured at the end of the incubation time by a

Tecan SpectraFluor plus microplate reader (excitation wavelength 485 nm; emission wavelength 530 nm). Data were normalized to the hydrogen peroxide-treated DMSO control and cell viability was assayed by a crystal violet staining, measured with a spectrophotometer at 590 nm. The number of viable cells was normalized to a DMSO control.

Cyclooxygenase inhibition assay

The COX inhibition assay was performed using the Cayman Chemicals COX Fluorescent Inhibitor Screening Kit according to the manufacturer's instructions. In this assay, arachidonic acid is converted to hydroperoxyl endoperoxide (PGG₂) by a COX component of the bifunctional enzymes COX-1 and COX-2. Followed by the reduction of PGG₂ to prostaglandin H₂ by the peroxidase component and 10-acetyl-3,7-dihydroxyphenoxazine (ADHP), highly fluorescent resorufin is generated. Its fluorescence can be measured with an extinction wavelength of 535 nm and an emission wavelength of 595 nm. In brief, ovine COX-1 or human recombinant COX-2 enzymes were incubated with *Tm*-PxB-1, *Tm*-PxB-4, CGA, or IQ in different concentrations, or buffer as a positive control with 100% initial COX activity, for 5 min. Wells without enzymes served as the negative control. The fluorescence intensity was measured 2 min after adding arachidonic acid. After subtracting the negative control, percentages of initial activities were normalized towards the positive control with 100% initial activity. IC₅₀ values were calculated by nonlinear regression analysis utilizing GraphPad Prism 9.

Cell treatment for Western blot and cytotoxicity analysis

J77A.1 cells were detached with accutase for an incubation time of 20 min. Then, 2 \times 10⁵ HeLa cells/well in 1000 μ L were seeded in 12-well plates and were allowed to attach for 24 h. Cells were stimulated with LPS (0.5 μ g/mL) and compounds as indicated for 4 h.

Western blot analysis

For cell lysis, cells were washed twice with ice-cold PBS. Then, 100 μ L of lysis buffer (50 mM Tris/HCl, 150 mM NaCl, 1% Nonidet NP-40, 0.25% sodium deoxycholate, 0.1% SDS) were added and lysates were frozen at -80 °C until further use. Lysates were thawed on ice and centrifuged (14000 rpm, 10 min, 4 °C) to remove cell debris. Protein concentrations were quantified by the Bradford assay and protein concentrations were quantified by linear regression analysis with BSA dilutions as protein standards. To adjust protein concentrations, each sample was diluted with SDS. Proteins were denatured at 95 °C for 5 min and were separated by SDS-PAGE in electrophoresis buffer (100 V, 21 min then 200 V, 43 min) on discontinuous polyacrylamide gels. Gels were combined by a gradient separation gel (4–20%) and a stacking gel. By tank blotting (100 V, 90 min, 4 °C), proteins were transferred to polyvinylidene difluoride (PVDF) membranes that were equilibrated before in tank buffer. Afterwards, membranes were blocked with 5% nonfat dry milk powder in PBS for 2 h. Primary antibody was added overnight at 4 °C (1 : 1000). Membranes were washed four times with TBS-T for 5 min each, before the secondary HRP-coupled antibody was added for 2 h (1 : 1000). A four-time washing procedure was repeated prior to the incubation with

ECL solution and chemiluminescence detection with a ChemiDoc Touch Imaging System. By comparison with Page Ruler Plus Prestained Protein Ladder, bands were assigned. Protein levels were analyzed by Image Lab Software and were normalized to the total protein level.

Cytotoxicity determination

In parallel, cell viability under the conditions of the Western blot experiment was assessed by two methods: (1) treated cells were washed with PBS, detached with 200 μ L accutase for 20 min, then diluted with 500 μ L culture medium; (2) 350 μ L of the cell suspension were transferred into a ViCell XR cell counter and cell viability was measured by trypan blue staining. Additionally, the same amount of cell suspension was used for flow cytometry. Therefore, cells were centrifuged (1000 rpm, 5 min, 4 °C) in precooled FACS tubes, washed twice with ice-cold PBS, and resuspended in 200 μ L PBS. Directly after, cells were kept in the dark on ice while flow cytometric analysis was conducted on a BD FACS Canto II (BD Biosciences). To determine viable cells in the samples, cells were gated for the living cells in the DMSO control by forward scatter (FCS) and side scatter (SSC) using FlowJo 7.6 software (BD Biosciences).

Statistical analysis

Results display the mean of at least three independent experiments (mean \pm standard deviation), each replicated in at least three repeats, if not stated otherwise. Statistical significance was calculated by one-way analysis of variance with post hoc analysis using Dunnett's multiple comparison test. All statistical analyses were performed with GraphPad Prism 9.

Supporting information

UV/Vis data and MS² fragmentations of all PxBs as well as NMR spectra of Tm-PxB-1,-2,-4 are available as Supporting Information.

Contributors' Statement

Conception and design of the work: SM, AV, TM; data collection PF, CN; analysis and interpretation of the data: PF, CN, AV, TM, SM; statistical analysis: PF, CN; drafting the manuscript: PF, CN, AV, TM, SM; critical revision of the manuscript: PF, CN, AV, TM, SM.

Funding

S. M. gratefully acknowledges funding from the Deutsche Forschungsgemeinschaft (DFG, German Research Foundation; Project-ID 448289381).

Acknowledgements

We would like to thank Dr. Lars Allmendinger and Claudia Glas for NMR measurements, and Dr. Andreas Gröger of the botanical garden Nymphenburg for his support in providing plant material and Dr. Cornelia Karg for help with data evaluation. We are deeply grateful to the Daumann Lab of LMU for providing access and support for the LC-MS measurements.

Conflict of Interest

The authors declare that they have no conflict of interest.

References

- [1] Wang P, Karg CA, Frey N, Frädrieh J, Vollmar AM, Moser S. Phyllobilins as a challenging diverse natural product class: Exploration of pharmacological activities. *Arch Pharm* 2021; 354: e2100061
- [2] Kräutler B. Phyllobilins – The abundant bilin-type tetrapyrrolic catabolites of the green plant pigment chlorophyll. *Chem Soc Rev* 2014; 43: 6227–6238
- [3] Moser S, Ulrich M, Müller T, Kräutler B. A yellow chlorophyll catabolite is a pigment of the fall colours. *Photochem Photobiol Sci* 2008; 7: 1577–1581
- [4] Vergeiner C, Ulrich M, Li C, Liu X, Müller T, Kräutler B. Stereo- and regioselective phyllobilane oxidation in leaf homogenates of the peace lily (*Spathiphyllum wallisii*): hypothetical endogenous path to yellow chlorophyll catabolites. *Chem Eur J* 2015; 21: 136–149
- [5] Erhart T, Vergeiner S, Kreutz C, Kräutler B, Müller T. Chlorophyll breakdown in a fern – Discovery of carbon-skeleton rearranged phyllobilin isomers. *Angew Chem Int Ed* 2018; 57: 14937
- [6] Li C, Wurst K, Berghold J, Podewitz M, Liedl KR, Kräutler B. Pyro-phyllobilins: Elusive chlorophyll catabolites lacking a critical carboxylate function of the natural chlorophylls. *Chem Eur J* 2018; 24: 2987–2998
- [7] Moser S, Erhart T, Neuhauser S, Kräutler B. Phyllobilins from senescence-associated chlorophyll breakdown in the leaves of Basil (*Ocimum basilicum*) show increased abundance upon herbivore attack. *J Agric Food Chem* 2020; 68: 7132–7142
- [8] Mathesius U. Flavonoid functions in plants and their interactions with other organisms. *Plants (Basel)* 2018; 7: 30
- [9] Faizal A, Geelen D. Saponins and their role in biological processes in plants. *Phytochem Rev* 2013; 12: 877–893
- [10] Dixon RA. Natural products and plant disease resistance. *Nature* 2001; 411: 843–847
- [11] Hayes M, Ferruzzi MG. Update on the bioavailability and chemopreventive mechanisms of dietary chlorophyll derivatives. *Nutr Res* 2020; 81: 19–37
- [12] Vaňková K, Marková I, Jašprová J, Dvořák A, Subhanová I, Zelenka J, Novosádová I, Rasl J, Vomastek T, Sobotka R, Muchová L, Vitek L. Chlorophyll-mediated changes in the redox status of pancreatic cancer cells are associated with its anticancer effects. *Oxid Med Cell Longev* 2018; 2018: 4069167
- [13] Karg CA, Taniguchi M, Lindsey JS, Moser S. Phyllobilins – Bioactive natural products derived from chlorophyll – Plant origins, structures, absorption spectra, and biomedical properties. *Planta Med* 2023; 89: 637–662
- [14] Karg CA, Wang P, Vollmar AM, Moser S. Re-opening the stage for *Echinacea* research – Characterization of phylloxanthobilins as a novel anti-oxidative compound class in *Echinacea purpurea*. *Phytomedicine* 2019; 60: 152969
- [15] Karg CA, Doppler C, Schilling C, Jakobs F, Dal Colle MCS, Frey N, Bernhard D, Vollmar AM, Moser S. A yellow chlorophyll catabolite in leaves of *Urtica dioica* L.: An overlooked phytochemical that contributes to health benefits of stinging nettle. *Food Chem* 2021; 359: 129906
- [16] Berg D, Youdim MB, Riederer P. Redox imbalance. *Cell Tissue Res* 2004; 318: 201–213
- [17] Stocker R, John F, Keane J. Role of oxidative modifications in atherosclerosis. *Physiol Rev* 2004; 84: 1381–1478
- [18] Behl T, Kaur I, Kotwani A. Implication of oxidative stress in progression of diabetic retinopathy. *Surv Ophthalmol* 2016; 61: 187–196
- [19] Toledo-Ibelle P, Mas-Oliva J. Antioxidants in the fight against atherosclerosis: Is this a dead end? *Curr Atheroscler Rep* 2018; 20: 36

- [20] Karg CA, Parráková L, Fuchs D, Schennach H, Kräutler B, Moser S, Gostner JM. A chlorophyll-derived phylloxanthobilin is a potent antioxidant that modulates immunometabolism in human PBMC. *Antioxidants (Basel)* 2022; 11: 2056
- [21] Jakubczyk K, Janda K, Watychowicz K, Aukasiak J, Wolska J. Garden nasturtium (*Tropaeolum majus* L.) – a source of mineral elements and bioactive compounds. *Rocz Panstw Zakl Hig* 2018; 69: 119–126
- [22] Gasparotto Junior A, Prando TB, Leme Tdos S, Gasparotto FM, Lourenço EL, Rattmann YD, Da Silva-Santos JE, Kassuya CA, Marques MC. Mechanisms underlying the diuretic effects of *Tropaeolum majus* L. extracts and its main component isoquercitrin. *J Ethnopharmacol* 2012; 141: 501–509
- [23] Gasparotto Junior A, Gasparotto FM, Lourenço EL, Crestani S, Stefanello ME, Salvador MJ, da Silva-Santos JE, Marques MC, Kassuya CA. Antihypertensive effects of isoquercitrin and extracts from *Tropaeolum majus* L.: evidence for the inhibition of angiotensin converting enzyme. *J Ethnopharmacol* 2011; 134: 363–372
- [24] Kleinwächter M, Schnug E, Selmar D. The glucosinolate-myrosinase system in nasturtium (*Tropaeolum majus* L.): variability of biochemical parameters and screening for clones feasible for pharmaceutical utilization. *J Agric Food Chem* 2008; 56: 11165–11170
- [25] Gasparotto A jr., Boffo MA, Lourenço EL, Stefanello ME, Kassuya CA, Marques MC. Natriuretic and diuretic effects of *Tropaeolum majus* (Tropealaceae) in rats. *J Ethnopharmacol* 2009; 122: 517–522
- [26] Bazyłko A, Granica S, Filippek A, Piwowarski J, Stefańska J, Osińska E, Kiss AK. Comparison of antioxidant, anti-inflammatory, antimicrobial activity and chemical composition of aqueous and hydroethanolic extracts of the herb of *Tropaeolum majus* L. *Ind Crops Prod* 2013; 50: 88–94
- [27] Wakana D, Kato H, Momose T, Sasaki N, Ozeki Y, Goda Y. NMR-based characterization of a novel yellow chlorophyll catabolite, Ed-YCC, isolated from *Egeria densa*. *Tetrahedron Lett* 2014; 55: 2982–2985
- [28] Müller T, Vergeiner S, Kräutler B. Structure elucidation of chlorophyll catabolites (phyllobilins) by ESI-mass spectrometry – pseudo-molecular ions and fragmentation analysis of a nonfluorescent chlorophyll catabolite (NCC). *Int J Mass Spectrom* 2014; 365–366: 48–55
- [29] Berghold J, Breuker K, Oberhuber M, Hörtensteiner S, Kräutler B. Chlorophyll breakdown in spinach: On the structure of five nonfluorescent chlorophyll catabolites. *Photosynth Res* 2002; 74: 109–119
- [30] Moser S, Müller T, Holzinger A, Lütz C, Kräutler B. Structures of chlorophyll catabolites in bananas (*Musa acuminata*) reveal a split path of chlorophyll breakdown in a ripening fruit. *Chemistry* 2012; 18: 10873–10885
- [31] Kuai B, Chen J, Hörtensteiner S. The biochemistry and molecular biology of chlorophyll breakdown. *J Exp Bot* 2017; 69: 751–767
- [32] Liu J, Wang H, Manicke NE, Lin JM, Cooks RG, Ouyang Z. Development, characterization, and application of paper spray ionization. *Anal Chem* 2010; 82: 2463–2471
- [33] Liu J, Wang H, Cooks RG, Ouyang Z. Leaf spray: direct chemical analysis of plant material and living plants by mass spectrometry. *Anal Chem* 2011; 83: 7608–7613
- [34] Apak R, Güçlü K, Demirata B, Özyürek M, Çelik SE, Bektaşoğlu B, Berker KI, Özyurt D. Comparative evaluation of various total antioxidant capacity assays applied to phenolic compounds with the CUPRAC assay. *Molecules* 2007; 12: 1496–1547
- [35] Li X, Jiang Q, Wang T, Liu J, Chen D. Comparison of the antioxidant effects of quercitrin and isoquercitrin: Understanding the role of the 6"-OH group. *Molecules* 2016; 21: 1246
- [36] Conrad A, Biehler D, Nobis T, Richter H, Engels I, Biehler K, Frank U. Broad spectrum antibacterial activity of a mixture of isothiocyanates from nasturtium (*Tropaeoli majoris* herba) and horseradish (*Armoracia rusticanae* radix). *Drug Res (Stuttg)* 2013; 63: 65–68
- [37] Lee EH, Park HJ, Jung HY, Kang IK, Kim BO, Cho YJ. Isoquercitrin isolated from newly bred Green ball apple peel in lipopolysaccharide-stimulated macrophage regulates NF- κ B inflammatory pathways and cytokines. *3 Biotech* 2022; 12: 100
- [38] Gerhäuser C. 68 – Phenolic Beer Compounds to Prevent Cancer. In: Preedy VR, editor. *Beer in Health and Disease Prevention*. San Diego: Academic Press; 2009: 669–684
- [39] Strohal M, Kavan D, Novák P, Volný M, Havlíček V. mMass 3: A cross-platform software environment for precise analysis of mass spectrometric data. *Anal Chem* 2010; 82: 4648–4651
- [40] Moser S, Scherzer G, Kräutler B. On the nature of isomeric nonfluorescent chlorophyll catabolites in leaves and fruit – A study with a ubiquitous phylloleucobilin and its main isomerization product. *Chem Biodivers* 2017; 14: e1700368
- [41] Karg CA, Wang P, Kluibenschedl F, Müller T, Allmendinger L, Vollmar AM, Moser S. phylloxanthobilins are abundant linear tetrapyrroles from chlorophyll breakdown with activities against cancer cells. *European J Org Chem* 2020; 2020: 4499–4509